Aircraft Observations of Boundary Layer Rolls off the Coast of California

IAN M. BROOKS AND DAVID P. ROGERS

Scripps Institution of Oceanography, La Jolla, California

(Manuscript received 1 February 1996, in final form 24 January 1997)

ABSTRACT

Large-scale horizontal rolls can have a significant influence on turbulent transport across the atmospheric boundary layer. The formation and maintenance of such rolls is dependent on the thermal and dynamic stability of the boundary layer (BL). The authors present aircraft observations of boundary layers, both with and without roll circulations, off the coast of California. The contribution of the rolls to the turbulent fluxes of heat, moisture, and momentum, and the variances of the three velocity components are determined for four cases. The fractional roll contributions to the u and w variances, and the sensible heat and along-wind momentum fluxes, show a near linear increase with altitude, from less than 10% at 30 m to more than 70% at the top of the BL. The variance in v and crosswind momentum flux are more scattered, although the variance shows a slight increase with altitude from about 40% to 60%. The latent heat flux also shows a great deal of scatter, especially in the lower third of the BL where the total flux is small; above this, values range between about 40% and 85% but show no clear trends. A stability parameter in the form of a bulk Richardson Ri number is calculated for each of 13 profiles through the boundary layer; it is found that the Richardson number successfully identifies those cases where rolls are present, and its value corresponds to some extent with the strength of the rolls. Values close to zero correspond to cases with well-defined rolls; for $0.1 < \text{Ri} < 0.25$ rolls are found to exist, but they tend to be weak and patchy; and no rolls are found where Ri is greater than the critical value of approximately 0.25. Reynolds numbers are calculated from a number of different definitions and indicate the dynamic instability of the shear dominated boundary layers.

1. Introduction

The existence of horizontal rolls in the atmospheric boundary layer (BL) has been known for many years; Woodcock (1941) inferred such convective patterns from the soaring behavior of seagulls, and they are frequently made manifest by the formation of lines or streets of clouds above their updraft regions. During the past 20–30 years, such secondary circulations have been the subject of much research, first as a purely dynamical phenomenon associated with instabilities in atmospheric flows and, more recently, as a major influence on turbulent transport within the atmospheric boundary layer. It is found that the roll scale may account for a significant fraction of the total fluxes. LeMone (1973) found that much of the heat flux in the upper 80% of the BL over land was due to rolls. Brümmer's (1985) results in a near neutral marine atmospheric boundary layer similarly show that the larger part of the heat flux in the upper BL is due to rolls. Chou and Ferguson (1991) found that rolls accounted for almost all of the heat and moisture transport at the top of a more convective BL during the Generation of Atlantic Lows Experiment, while in the lower half of the BL smaller scales dominated and the rolls accounted for less than 25% of the flux (Chou and Zimmerman 1989). In all cases the influence of the rolls is found to increase with altitude, their fractional contributions to the total fluxes being small near the surface. LeMone (1976) also found that the small-scale turbulence is modulated by the roll circulations, being concentrated in the updraft regions of the flow. It is not obvious from these studies whether the presence of rolls leads to an enhancement of fluxes or simply a redistribution of the flux contributions between scales. Relatively little work appears to have been done on this question, but there is some evidence that rolls may lead to enhanced fluxes. Chou (1993) compared a number of bulk flux parameterizations and direct eddy correlation fluxes and found that the bulk schemes tended to underestimate the momentum flux in the presence of rolls. Extensive reviews of most of these studies are to be found in Brown (1980) and Etling and Brown (1993), along with a basic description of the theoretical background. Etling and Brown (1993) note that rolls are ubiquitous under favorable conditions. The frequency and extent of such conditions can be judged by the fact that satellite imagery of the eastern Pacific, coinciding with the research flights from which our data is drawn, show cloud streets somewhere off the coast on every

Corresponding author address: Dr. Ian Brooks, Scripps Institution of Oceanography, University of California, 9500 Gilman Drive, La Jolla, CA 92093-0230.
E-mail: brooks@myfanwy2.ucsd.edu

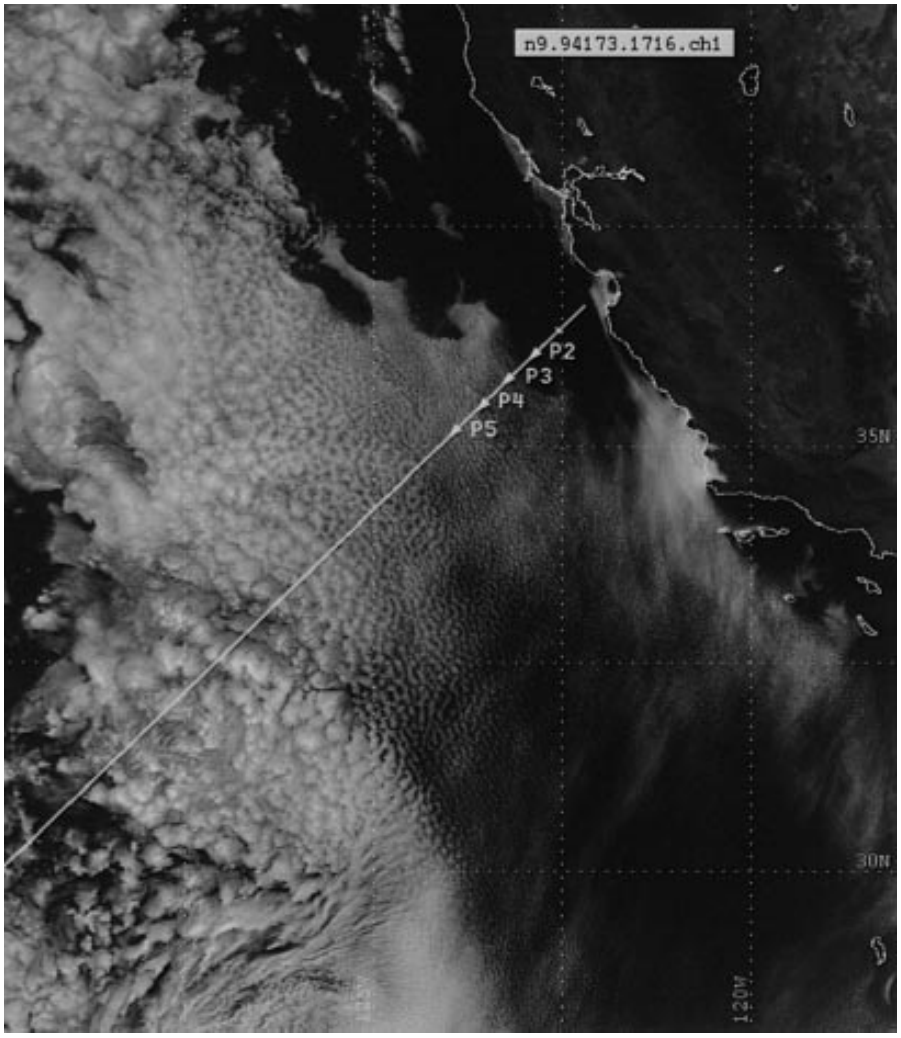

FIG. 1. NOAA-9 AVHRR channel-1 (visible) image for 22 June, 1716 UTC showing cloud bands off the western coast of the United States. Grid lines are at 2.5° intervals. The solid line shows the flight track of the aircraft as it made a series of profiles moving away from the coast; from the edge of the cloud to a position of approximately 35.4°N, 123.7°W the aircraft made several profiles (P2–P4) through rolls before moving into a cellular convection regime as the boundary layer deepened and became more convective. Arrowheads mark the end of each consecutive profile. Note that while the last indicated profile (P5) appears to be just within the roll regime, observations from the aircraft indicate that this was not the case. The discrepancy is due to the time interval between the image and latter part of P5 within the boundary layer (9 min) and to potential errors of several kilometers in the navigation of the satellite image.

day (Fig. 1), although not necessarily in our region of operations.

Since large-scale, secondary circulations are widespread over the oceans and make significant contributions to the turbulent transport of heat, moisture, and momentum across the boundary layer, it is important that we fully understand their behavior, the conditions under which they form, and their contribution to transport processes in order to include their effects in large-scale models where turbulent transport must be parameterized. A simple criteria indicating the presence of rolls is of considerable use in this context. Deardorff (1972) related the flow in an early 3D large eddy simulation (LES) model of neutral and convective boundary layers to the stability parameter z_i/L, where z_i is the inversion height and L is the Obukhov length, defined as

$$L = \frac{-\overline{\theta_v} u_*^3}{kg(\overline{w'\theta_v'})_0}, \tag{1.1}$$

where θ_v is virtual potential temperature, u_* is the friction velocity $= (\overline{w'u'}_0^2 + \overline{w'v'}_0^2)^{1/2}$, k is the von Kármán constant, and g is gravitational acceleration; zero subscripted terms are surface values. He found that for the neutral and weakly unstable boundary layers ($z_i/L \geq$

-4.5) turbulent eddies tended to become elongated by the mean wind shear and form rolls, while for a strongly unstable BL ($z_i/L < -10$), the ordering effect of the wind shear gave way to the random orientation of convective plumes. LeMone (1973) presented observations of rolls from several land-based field studies under a variety of conditions and found rolls for $-3 > z_i/L > -10$; a similar range was found by Chou and Ferguson (1991) over the ocean with $-4 > z_i/L > -11$. Walter and Overland (1984) made aircraft and satellite observations of steam fog formed over cracks and leads in sea ice with $z_i/L = -1.2$. They found roll vortices at several different scales, the interaction of which produced organization of the fog on scales between 2 and 30 km. Moeng and Sullivan (1994) carried out LES simulations of four boundary layers including the extremes of shear and buoyancy forcing, and two intermediate cases. They used the ratio of u_* to the convective velocity w_* as a measure of stability, where

$$w_* = \left[\frac{g z_i (\overline{w'\theta'_v})_0}{\overline{\theta}_v}\right]^{1/3}. \tag{1.2}$$

They investigated only the shear limit on roll formation and found $u_*/w_* < 0.65$ ($z_i/L < -1.5$). They compared this criterion with that found by Sykes and Henn (1989) in their simulation of heated channel flow. This is a source of potential confusion since the Sykes and Henn criterion of $u_*/w_* > 0.35$ ($z_i/L > -9.3$) relates to the buoyancy limit on roll formation. The variability in the proposed shear and buoyancy limits of the criteria suggest that z_i/L alone may be an inadequate indicator of conditions in which rolls are supported.

Kelly (1984) calculated the Richardson, Raleigh, and Reynolds numbers for BL rolls over Lake Michigan. Although conditions were highly convective throughout, he sampled a wide range of roll depths and aspect ratios, correlation of which with the Richardson and Rayleigh numbers suggested that in spite of the strong convective forcing, shear instability might be the more important factor in determining roll geometry. Brümmer (1985) studied three cases of rolls over the North Sea under near neutral conditions ($z_i/L > -2$) in which he tried several definitions of the Richardson number in order to find which would best identify the stability of the BL with respect to rolls. The principal forcing was determined from an analysis of roll-scale kinetic energy budget terms and related to various definitions of the Reynolds number. While definitions of Ri and Re that successfully diagnosed the three roll cases and the mechanism supporting them were determined, these stability conditions still require testing against a larger dataset, including cases without roll circulations. This paper presents the results of such a test. A detailed discussion of the stability parameters and their definitions are given in section 5.

The data presented here were collected by the C-130 *Hercules* aircraft of the U.K. Meteorological Office's

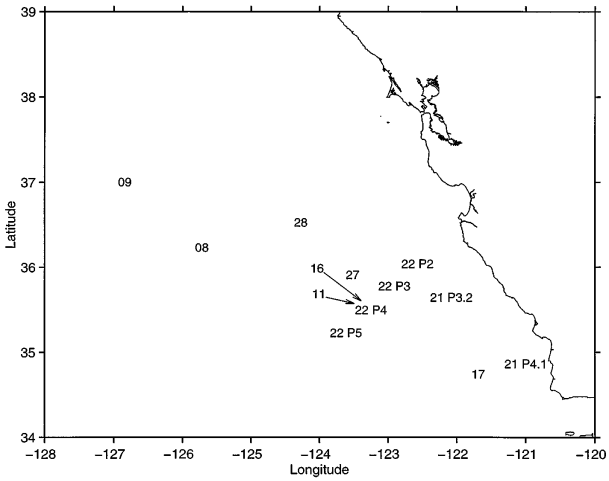

FIG. 2. The region of aircraft operations off the coast of California. The numbers refer to the dates in June 1994 of the cases used in this study and show the approximate location of each profile.

Meteorological Research Flight (MRF) during June 1994 while participating in the Monterey Area Ship Tracks experiment (MAST) off the coast of California (Fig. 2). While the experiment was not primarily concerned with boundary layer dynamics, some of the turbulence measurements clearly indicated the influence of large-scale secondary circulations within the BL. Most field studies of roll circulations have been made under conditions where strong, coherent circulations are maintained over relatively large areas, namely, cold air outbreaks over the oceans where conditions are highly convective (Kelly 1984; Hein and Brown 1988; Chou and Ferguson 1991). In the present study the boundary layer was near neutral ($z_i/L > -2.3$) or, on occasion, slightly stable, and in many cases the rolls were found only in a relatively narrow region off the coast, typically of the order of 100 km or so. Farther west, the BL deepened as conditions became more convective and rolls gave way to disordered thermal plumes. Figure 1 illustrates the extent of rolls on 22 June where banded cloud structures are visible for 200–300 km off the coast. It should be emphasized that the cloud streets by which the rolls are made visible are a result of the circulation but are not essential for its maintenance. The latent heat released along the cloud streets may, however, add to strength of the circulations (Chlond 1992). Several of the cases presented here have rolls spanning areas with and without clouds, and it is probable that the rolls on 22 June extend into the clear air to the north and south. Another important observation is the large-scale structure or distribution of the rolls. A range of roll scales are evident in the spacing of cloud bands, and individual rolls are of relatively limited along-wind extent, frequently merging and changing orientation. This is in contrast to the more regular, coherent organization and greater along-wind extent of rolls formed in cold air outbreaks (Brown 1980, Figs. 1 and 2). This organi-

zation is typical of the roll cases observed in this study and is clearly a common and widespread phenomenon. A similar structure is observed in a recent LES modeling study under comparable conditions (Glendening 1997). The availability of a range of cases in this study, both with and without rolls, provides an excellent dataset with which to test stability criteria as predictors of roll circulations and assess the roll-scale contribution to the transport of heat, moisture, and momentum.

2. Data collection

The C-130 is instrumented to make measurements of a wide variety of meteorological, dynamical, radiative, and microphysical variables. The standard instrumentation is well documented (Rogers et al. 1995) and will not be described in great detail here. The three wind components are derived from a pitot-static pressure system at the tip of the aircraft's nose boom in conjunction with two wind vanes, or gust probes, situated just behind the tip of the boom. Aircraft motions are monitored by an inertial navigation unit (INU), which is corrected by comparison with a global positioning system (GPS) to remove the Schuler oscillations and long period drifts common in INU systems. The temperature measurements used in this paper are derived from the MRF in-cloud temperature probe (ICTP), a 4.3-μm CO_2 absorption band radiation thermometer. This is used in preference to the Rosemount platinum resistance thermometers because it does not suffer from wetting problems in cloud, which causes problems with the determination of the heat flux in broken cloud layers. Dew point temperature and total water mixing ratio are measured by a Lyman-α absorption hygrometer, which is calibrated against a General Eastern cooled mirror hygrometer during runs in clear air. Liquid water content (LWC) is measured by a Johnson–Williams hot wire probe and cloud droplet spectra by a particle measuring systems forward scattering spectrometer probe (FSSP).

The overall flight patterns used during MAST were determined by the primary aim of investigating the microphysical changes in cloud caused by the presence of an exhaust plume from a ship. Although the characterization of the boundary layer turbulence structure was an integral part of the primary experimental aims, other operational considerations determined when and where turbulence stacks were made, with the result that some of the flight legs are less than ideally situated for the study of roll circulations and much of the data used in this analysis are less detailed than we would have wished.

The cases included in this study are a subset of the measurements made during the MAST field project; they consist of all the profiles with closely associated stacks of turbulence runs, plus a number of additional profiles where the presence, or otherwise, of rolls was known with a high degree of confidence from observations noted in the flight scientist's log. The typical turbulence runs made during each flight were a series of 10-min horizontal flight legs (approximately 60 km at a nominal airspeed of 100 m s^{-1}) across the mean wind and stacked vertically, either above a fixed ground position or maintaining relative position in the airmass by allowing the runs to drift with the wind. The lowest level run, visibility permitting, was made at an altitude of 30 m. Other run levels were chosen with reference to a vertical profile, made prior to the turbulence stack, from above the inversion down to 14 m above sea level; they typically include runs in the subcloud layer, near cloud base, just below cloud top, and above the inversion.

The identification of which cases have large-scale roll structures present may involve a number of stages, particularly where the crosswind extent of the rolls is limited or the wider cloud field very broken. The most direct form of identification is the direct observation of cloud streets, either from the aircraft or from satellite imagery. If the aircraft does not gain sufficient altitude, the banding of the cloud structure may not be obvious to the observers. The time series of downwelling shortwave radiation and cloud droplet concentration can help to identify banded clouds when the aircraft is below or in the cloud layer. The power spectra of these parameters are used to more clearly define the scales of the rolls from cloud band spacing (Fig. 3). The cospectra and associated Ogive curves—the running integral of cospectral density from high frequency to low—frequently show significant contributions at scales indicative of BL scale motions (Fig. 4). The cospectra alone cannot reveal whether a separation of turbulent transport over different scales is due to rolls or not, but they can help identify those cases where rolls may exist. Having identified possible roll cases, the phase and coherence spectra of the vertical and crosswind velocity components w and v provides confirmation (Fig. 5). A high coherence between w and v with a phase shift close to 90° is a clear indication of rolls, since randomly distributed convective plumes or waves have no such relationship (Hein and Brown 1988). Where the rolls are strongest, this behavior can be seen directly in the time series of w and v after filtering to remove high-frequency variability. The limited extent and relatively weak nature of some of the roll cases observed in this study, and the high variability in roll scale complicates the identification process, and there remains one borderline case (8 June) for which we have been unable to confidently decide one way or the other.

For those cases where turbulence statistics were to be calculated, the portions of flight track to be used were examined to ensure suitability. Sudden changes of aircraft attitude or heading can lead to spurious values in the wind measurements, and changes of altitude of more than 25 m or so can potentially lead to the sampling of different turbulent regimes, particularly where runs have been selected to lie close to the division between distinct layers identified from the preceding profile. In order for meaningful turbulent quantities to be

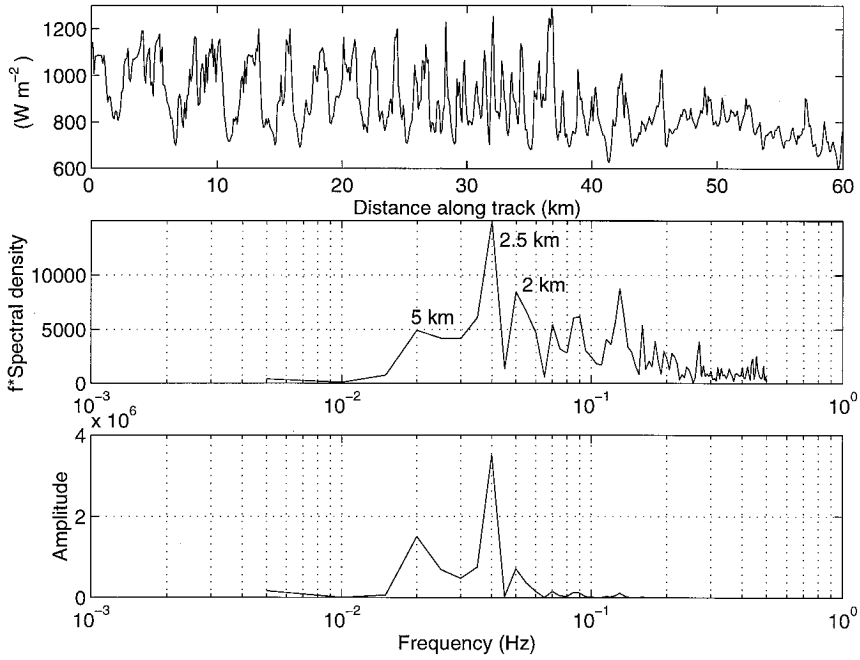

FIG. 3. Time series of the downwelling flux of visible radiation for a run near cloud base on 21 June and its frequency weighted spectral density, a maximum is visible at a frequency corresponding to a scale of approximately 2.5 km. Further maxima are present at smaller scales down to just under 1 km, approximately twice the BL depth. The amplitude spectra provides an indication of which peaks are statistically significant. These scales correspond closely with those of the rolls indicated by Fig. 6.

calculated the BL must be sufficiently stationary over the length of the flight leg. If the Ogive curve approaches asymptotically a single value, then this condition is met, and the final value of the Ogive represents the total covariance or flux (Fig. 4). The frequency (scale) below (above) which negligible change occurs defines the averaging interval required to capture all frequency contributions to the flux. The Ogive in Fig. 4 is from a case with rolls (21 June) and displays two discernible ranges. The curve first flattens out at approximately 0.13 Hz (0.77 km); this is the low-frequency limit of the small-scale turbulence. Below 0.08 Hz (1.25 km) the flux contributions increase again and the Ogive increases before finally flattening out by 0.02 Hz (5 km). This lower range of frequencies corresponds to the roll-scale contributions to the flux. The small-scale and roll-scale fluxes are selected by integration of the cospectra over the frequency ranges from 16 Hz to a cutoff frequency of approximately 0.1 Hz and from the cutoff frequency down to approximately 0.02 Hz. The precise low-frequency cutoff for turbulent contributions is chosen to lie in the spectral gap between the scales. It is estimated directly from the broad minima in the cospectra and checked for consistency across all the flight legs in the stack, with the phase spectra and cloud band spacing. Provided that an identifiable division exists between the turbulence and roll scales and the averaging length is sufficient, this technique is relatively insensitive to the precise details of flight leg and averaging lengths. In some cases, real boundary layer data do not meet the condition of stationarity and the Ogive curves do not approach a single value. Interpretation of the data becomes more difficult in these cases. Inspection of the profiles of mean quantities to identify the depths of distinct layers may allow realistic upper limits to be set for scales contributing to turbulent transport. Other techniques may be required to identify other phenomena that may contaminate the turbulence data, such as gravity waves. The use of Ogive curves when estimating fluxes provides a useful insight into turbulence structure since they give a detailed picture of how different scales contribute to turbulent transport.

When scale partitioning the fluxes, it is inevitable that any nonroll turbulence on scales similar to the rolls will be included with the roll fraction. In the present case we believe that any such contribution from individual eddies will be small. The cospectra and Ogive curves (Fig. 4) show a distinct spectral gap. A more continuous spectrum would be expected if significant 3D turbulence extended up to the scale of the rolls. When carrying out a similar scale partitioning, Chou and Ferguson (1991) explicity assume, 3D plumes to occupy scales smaller than that of the observed rolls. Coherence spectra (Fig. 5) suggest that the roll-scale structures observed have a relatively high coherence over scales of tens of kilometers; this would not be the case for randomly dis-

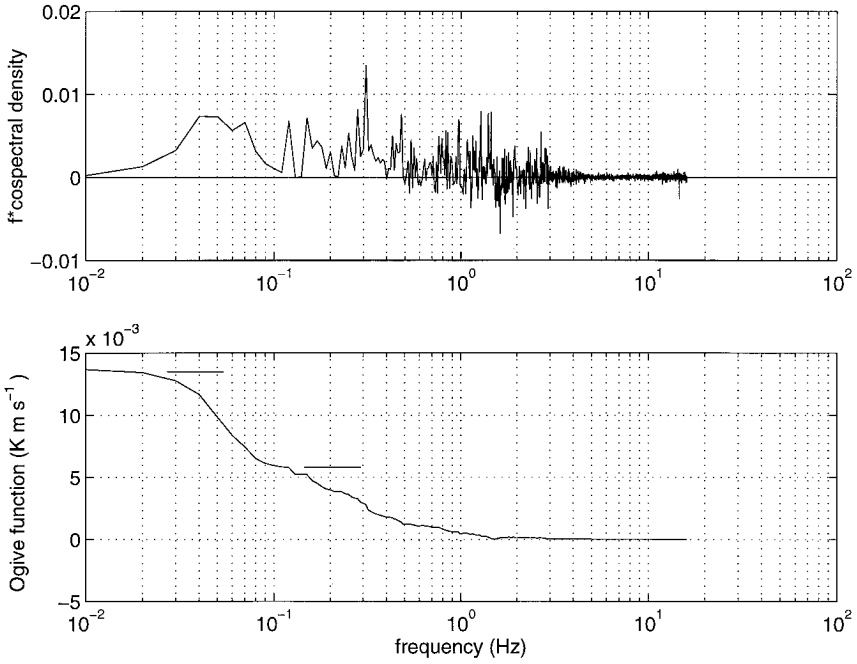

FIG. 4. An example of the frequency-weighted cospectral density and ogive function for $\overline{w'\theta'}$ for a run at 250 m on 21 June 2007–2018 UTC, between 35.64°N, 122.47°W and 35.87°N, 121.87°W, associated with profile P3.2. The horizontal bars indicate the values of the small-scale and total heat fluxes; the difference between the two is attributed to the roll-scale contribution. The cutoff for the high-frequency contributions is chosen to lie in the spectral gap that can be seen between the small- and roll-scale contributions to the total transport. Given the nominal airspeed of 100 m s^{-1}, spatial scales can be determined from the frequency scale as scale in km = 0.1/frequency, so that 10^{-2} = 10 km, 10^{-1} = 1 km, etc.

tributed turbulent eddies of a similar size. An alternative approach to partitioning the fluxes is to create composite rolls by averaging together sections of the time series corresponding to one roll wavelength, thus averaging out nonroll turbulence in the same spectral range (LeMone 1973). This approach requires the assumption of uniform roll spacing, as is approximately the case in moderately convective conditions. In the present case the roll spacing is observed to vary by up to a factor of 5, invalidating the assumption that permits the compositing of the rolls.

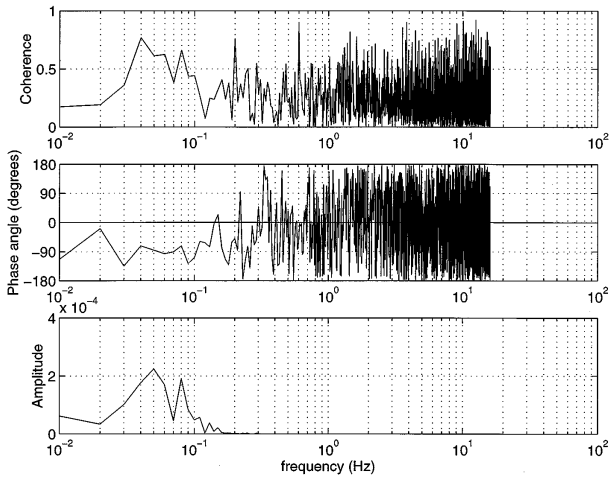

FIG. 5. Coherence and phase spectra for the vertical and crosswind velocity components w and v for a run in cloud (at 310 m) on 21 June (P3.2). The high correlation and near 90° phase angle between 1 and 2.5 km (indicated by the horizontal bars) clearly indicate the presence of rolls on these scales. The amplitude spectrum indicates the statistical significance of the phase and coherence spectra.

Prior high-pass filtering of the individual time series is unnecessary since averaging and integration of the cospectra over specific frequency ranges amounts to the selective filtering out of low-frequency contributions to the covariance. The ICTP temperature measurements, and the horizontal u- and v-wind components are low-pass filtered to attenuate excessive noise at high frequencies. This noise does not contribute significantly to the turbulent fluxes since it is uncorrelated with w but can cause problems with the calculation of velocity variances. The noise in u and v was intermittent, possibly resulting from a vibrational problem, and at a frequency of between 6 and 8 Hz. With the exception of the noise peak the contribution to the velocity variances from frequencies above approximately 3 Hz was negligible and so a filter was applied to attenuate all frequencies above this value. Most parameters are sampled at 32 Hz, and all turbulent quantities are calculated from data at this frequency, mean quantities are taken from 1-s averages.

TABLE 1. Geometric flow parameters. Here, H is the roll height, assumed equal to the BL depth, Z_{IP} is the altitude of the inflection point in the crosswind profile, BL wind orientation is given in degrees from north (clockwise is positive), the roll orientation is given with respect to the mean BL wind and has standard deviations of between 2° and 4°, and λ is the roll wavelength (mean and range) estimated from the distance between cloud streets as determined from the FSSP droplet concentration. The entry is blank when data is unavailable, a dash indicates that a parameter is not applicable. All altitudes are in meters. Times of profiles are given in UTC to the nearest minute.

Date Time UTC	Rolls?	$H(=Z_i)$	Cloud base	Z_{IP}	BL wind orientation	Roll orientation	λ (km)	λ/H
08:P2 2239–2245	?	580	320	580	−17.1		—	—
09:P1 2124–2130	Y	350	250	380	−4.7		1.4 (0.5–2.7)	4 (1.4–7.7)
11:P1 2037–2041	N	490	250	530	−2.4	—	—	—
16:P1 1608–1615	Y	740	450	675	−13.9	−9	1.7 (0.7–2.7)	2.3 (0.9–3.6)
17:P1 1742–1751	Y	610	500	625	−27.3	−3		
21:P3.2 1934–1838	Y	460	260	425	−28.8	−3	1.7 (0.9–3.1)	3.7 (1.9–6.7)
21:P4.1 2218–2224	Y	370	225	370	−41.7		1.0 (0.5–1.5)	1.9 (1.3–4.0)
22:P2 1656–1703	Y	510	375	520	−25.9			
22:P3 1703–1710	Y	510	400	520	−22.9	−6		
22:P4 1710–1718	Y	555	400	570	−23.2	−6		
22:P5 1718–1725	N	650	500	—	−17.5	—	—	—
27:P2 1945–1952	N	520	300	160	−27.9	—	—	—
28:P2 1853–1900	N	645	350	—	−10.7	—	—	—

3. Mean boundary layer conditions and roll characteristics

The synoptic conditions throughout most of the project were typical of those responsible for about half of the shallow stratocumulus-topped boundary layers in this region during the summer months (Brost et al. 1982; Rogers and Telford 1986). Winds were northerly and an extensive, although frequently broken, sheet of stratocumulus was observed off the coast on a more or less daily basis. Wind speeds were consistently high, typically of the order of 10–12 m s^{-1} near the surface and 12–16 m s^{-1} throughout the remainder of the boundary layer. Large shears were frequently observed at the inversion as well as near the surface. Nearshore winds were trapped by the coastal mountain range and tended to follow the coastline. Offshore flow was intermittently observed farther north, over Oregon and Washington; this tended to keep the nearcoast region clear of stratocumulus and forced many of the flights farther west. The inversion was low near the coast, typically about 500 m, but increased to the west. Inversion height varied widely from day to day, however, ranging from 300 to 1600 m. Upwelling cold water along the coast causes a large sea surface temperature (SST) gradient in the region of operations. The mean gradient is of the order of 1 K per 100 km, increasing to the southwest, but local gradients were observed to be very much larger and led to occasionally highly heterogeneous conditions. The air temperature tended to follow the SST and increase with distance from the coast. The air temperature was usually slightly less than the SST ($\theta_{\ell,air} - \theta_{\ell,SST} > -1$ K), resulting in generally weak surface buoyancy forcing. In a few cases the air was slightly warmer than the sea surface and the BL stable.

The variability of the BL depth may give rise to some concern as to the effect of the mesoscale processes associated with this variability on the observed rolls. The primary forcing affecting BL depth is the surface buoyancy flux, which is strongly dependent on the SST. While the general trend is for increasing SST offshore, the gradient is far from uniform, as noted above. Both the aircraft measurements and satellite retrievals reveal that there are large areas of near-uniform SST and sudden changes across relatively short distances—SST fronts. Similarly, the BL depth does not change uniformly but remains approximately constant over broad areas and increases rapidly some distance off the coast, as the BL becomes more convective over a warmer SST (Table 1, 22 June). The roll observations are confined to the shallow, near-uniform coastal BL. While the coastal BL exhibits considerable spatial variability, it is observed to change only slowly with time. The stationarity of the conditions is evidenced by the convergence of the Ogive curves at scales less than 10 km (e.g., Fig.

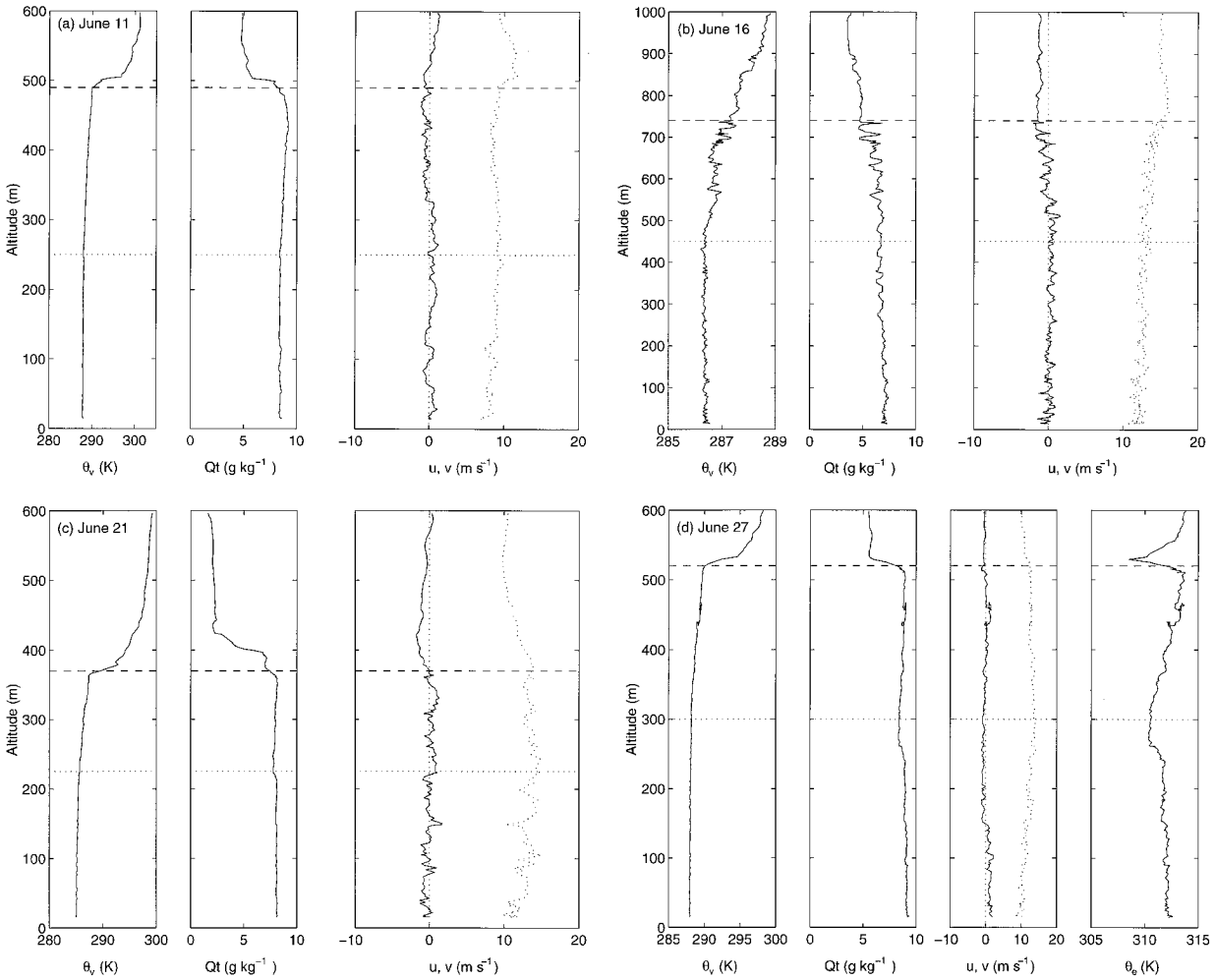

FIG. 6. Example profiles of virtual potential temperature θ_v, total water content Q_t, and the along- and cross-mean wind components u (dotted line) and v (solid line). Figure 4d also shows the equivalent potential temperature that more clearly shows the decoupling below cloud base. The horizontal dashed lines indicate cloud top (and roll top where rolls are present), the dotted lines indicate cloud base. The cases shown are (a) 11 June, (b)16 June, (c) 21 June P4.1, and (d) 27 June.

4). Thus, while mesoscale processes determine the distribution of the rolls, their effect upon the temporal evolution is small and should not unduly affect measurements made over a period of 1 h or less.

Figures 6a–d show four examples of typical profiles of virtual potential temperature θ_v, total water content Q_t, and the wind components u and v rotated into a coordinate system aligned with the mean boundary layer wind. Figure 6d additionally shows the equivalent potential temperature θ_e, which highlights the decoupling observed in this case. The profiles shown encompass two cases with rolls (Figs. 6b,c) and two without rolls (Figs. 6c, d). The horizontal dashed lines indicate cloud top, as identified from profiles of LWC or FSSP droplet concentration (not shown), and the dotted lines indicate cloud base. In all but three of the cases studied, the stratification of the subcloud layer is slightly unstable. Where surface buoyancy fluxes have been estimated, they are positive (in all cases a positive flux indicates transport upward). The remaining cases on 21 (P4.1), 22 (P2), and 27 June are all slightly stable, although the surface buoyancy flux on 21 June is positive. Some discrepancy between the profile and flux might be expected if the profile is contaminated by horizontal variability. The surface buoyancy flux on 27 June is negative, in agreement with the stability. No turbulence runs were made on 22 June. The 27 and 28 June cases both show signs of weak decoupling approximately 50 m below cloud base, indicated by a fall in Q_t, and θ_e at this level (Fig. 4d). Decoupling occurs where shortwave heating of the cloud layer offsets the longwave cooling at cloud top, stabilizing the cloud layer and impeding turbulent transfer between the surface and cloud layers (Rogers and Koracin 1992; Martin et al. 1995). Decoupling may inhibit the formation of rolls on the scale of the BL. It is, however, difficult to determine whether the decoupling in these cases is actually inhibiting the formation of rolls or if it has formed as a consequence

of the poor mixing across the BL in the absence of rolls. The profiles for 16 June (Fig. 4b) appear much noisier than for the other cases. This is largely due to the very weak inversion that allows a greater degree of entrainment of warm, dry air from above the BL than in the other cases. The variability is greatest near the top of the BL where the aircraft passes through regions of unmixed BL and free troposphere air; this is most clearly shown in the Q_t profile. Lower in the BL the air is better mixed and the variability reduced.

Many of the crosswind velocity profiles exhibit an inflection point at or near the inversion. It is often assumed that where an inflection point is present in the wind profile and conditions are near neutral, the secondary circulations are due to the inflection-point instability (Brümmer et al. 1982; Walter and Overland 1984). In such cases, the rolls derive their energy from the crosswind shear production near the inflection point; however, Raasch (1990) found that thermal forcing can still be important under these conditions and that the influence of the inflection point should not be overestimated if it is close to the top of the BL. Brümmer and Latif (1985) also found that the influence of the inflection point was reduced if it occurred above $0.6z_i$, and Brümmer's (1985) calculation of the roll-scale kinetic energy budget showed that one of his cases, previously assumed to be dynamically forced (Brümmer et al. 1982), was actually buoyancy driven. It is unlikely that the inflection points observed in the cases presented here correspond to any that may have been present before, and contributed to, roll formation. Mixing by the rolls modifies the mean flow, making identification of the original flow difficult or impossible.

Roll depth is generally assumed equal to the boundary layer depth (LeMone 1973; Etling and Brown 1993), although it is not necessarily so. Brümmer (1985) assumed roll depth equal to cloud-top height, and found this extended well into the deep, though relatively weak, stable inversion layer. We assume roll depth to be equal to the cloud-top height. In most cases this agrees closely with the base of the temperature inversion. The use of either measured cloud-top or inversion height may result in a small error. Broken cloud may be intercepted below its maximum altitude due to the shallow angle of the aircraft's descent during profiles, and the inversion is often perturbed by cloud-scale motions so that its measured altitude depends on the position at which the aircraft passes through it. In either case, the error is not large (typically a few percent) and does not significantly affect the calculations in section 5. It is common practice in studies of rolls to rotate the horizontal wind components into a coordinate system aligned with the roll axes. This has not in general been possible in the present study since the orientation of the rolls is not well defined. As a first approximation the coordinate system used is aligned with the direction of the mean BL wind. This is in any case a more generally applicable coordinate system to choose since one of our principal aims is to test stability parameters as indicators of the presence of rolls, assuming no prior knowledge of their existence.

Table 1 gives some geometric parameters of the flow: inversion height z_i, orientation of the mean wind, the height of any inflection point in the wind profile, the roll wavelength λ (when present), and aspect ratio λ/H. The observed roll height H is in general equal to the inversion height, and the roll wavelength is determined from the horizontal spacing of cloud bands. Where satellite imagery coincides closely with the observations, the orientation of cloud bands with respect to the mean wind has been estimated; the quoted values are averages over all the identifiable cloud bands in the vicinity of aircraft operations. The mean wavelengths (1–1.7 km), aspect ratios (1.9–4), and orientations of the rolls (3°–9° to the left of the mean flow) agree well with those from many previous studies (Kelly 1984).

4. Turbulence properties

Of the cases where rolls are present, only four have usable stacks of turbulence runs oriented across the mean wind and hence across the rolls. On 17 June the runs in the vicinity of the rolls are oriented too close to the roll axes to provide useful cross-roll turbulence statistics, while on 22 June there were no horizontal runs made at all. Figures 7a–d show the variances of the three wind components and profiles of total turbulent fluxes of sensible and latent heat, buoyancy, and momentum. The roll-scale contributions are overlaid. The roll-scale contributions are equal to the difference between the small scale and total fluxes (as indicated in Fig. 3), and equivalent to the integral of the cospectrum over the range of frequencies corresponding to the roll wavelengths, typically 2–8 times the BL depth. The vertical scales have been chosen to equal the roll depth. The latent heat fluxes should be regarded with caution since total values are very small and hence prone to large errors. Figures 8a–g show composite plots of the fractional roll-scale contributions to the variances and fluxes from all four cases.

The velocity variances show a number of common features. The total along-wind variance has a maximum near the surface and decreases rapidly with altitude; the position of the maximum in the roll scale contribution appears to vary, although its fractional contribution increases almost linearly with altitude. The cross-wind variances have a near surface maxima and generally decrease with altitude toward the middle of the BL. They differ somewhat in the upper BL; only the 21 June (P3.2) shows the second maxima expected for a roll circulation. On 9 and 21 June (P4.1), there is a lack of data in the upper BL, while on 16 June the variance continues to decrease with altitude throughout the BL depth. There is no clear pattern to the fractional roll contribution to $\overline{v'^2}$, although a slight increase with altitude may be discerned in the composite plot. The vertical velocity vari-

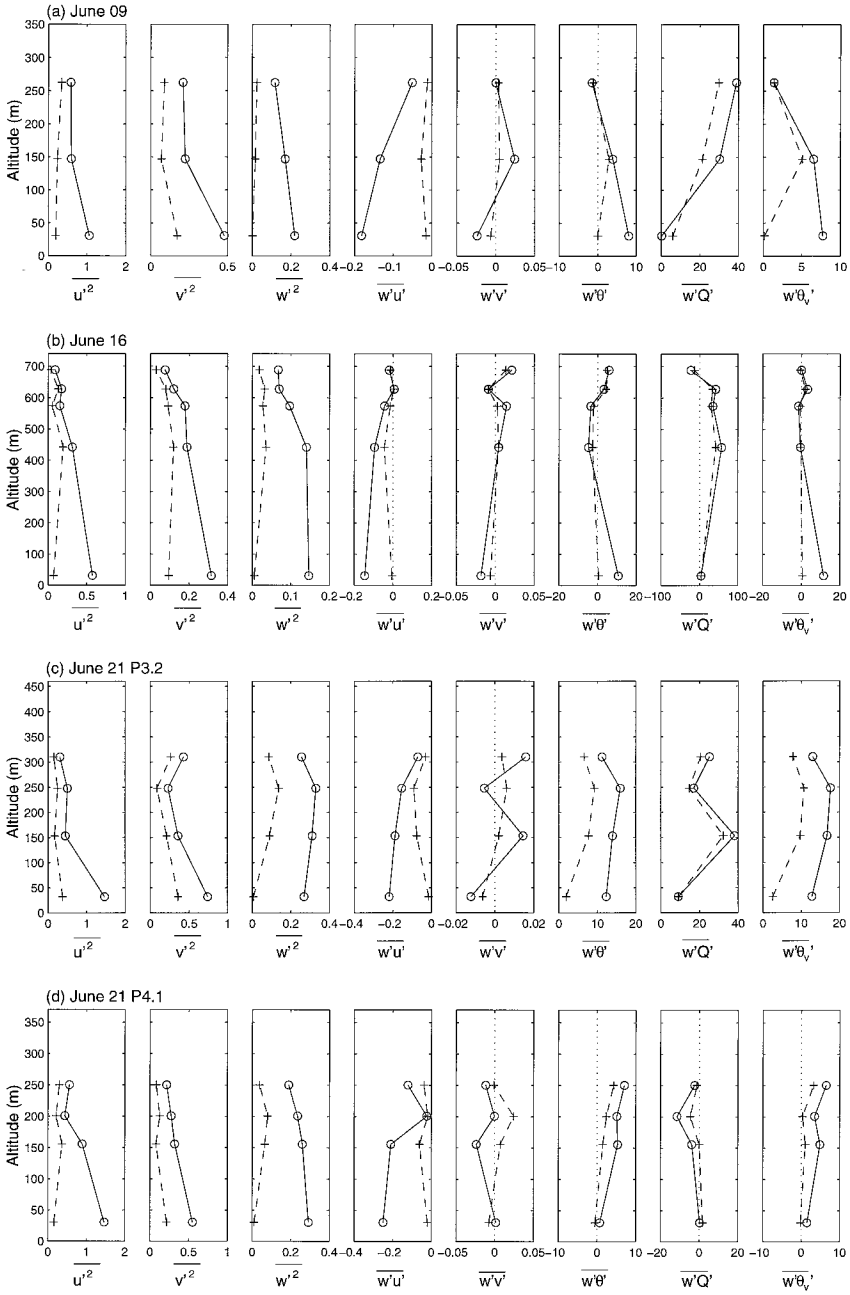

FIG. 7. Profiles of velocity variances and fluxes of momentum, heat, and moisture for the cases (a) 9 June, (b) 16 June, (c) 21 June P3.2, and (d) 21 June P4.1. Circles and solid lines show the total values, crosses and dashed lines indicate the roll scale contribution; the vertical scales are equal to the roll depth. Units: velocity variances in $m^2\ s^{-2}$, momentum fluxes in N m^{-2}, and heat and moisture fluxes in W m^{-2}.

ance tends to decrease with altitude from a near-surface maximum, although the P3.2 case on 21 June has a maxima higher in the BL, possibly due to the higher degree of convection in this case compared with the P4.1 and 9 June. The 16 June case is even more convective, but the lack of runs in the lower BL leaves the profile shape uncertain. The fractional contribution of the rolls increases from a minimum near the surface up to approximately the middle of the BL; above this there is a split between the cases. Both the 21 June cases suggest a decrease in the upper BL, while the 9 and 16 June cases show a continued increase.

The along-wind momentum flux exhibits a consistent general pattern across all four cases. The total flux decreases from a maximum at the surface, while the roll-scale contribution is near zero at the surface and at a

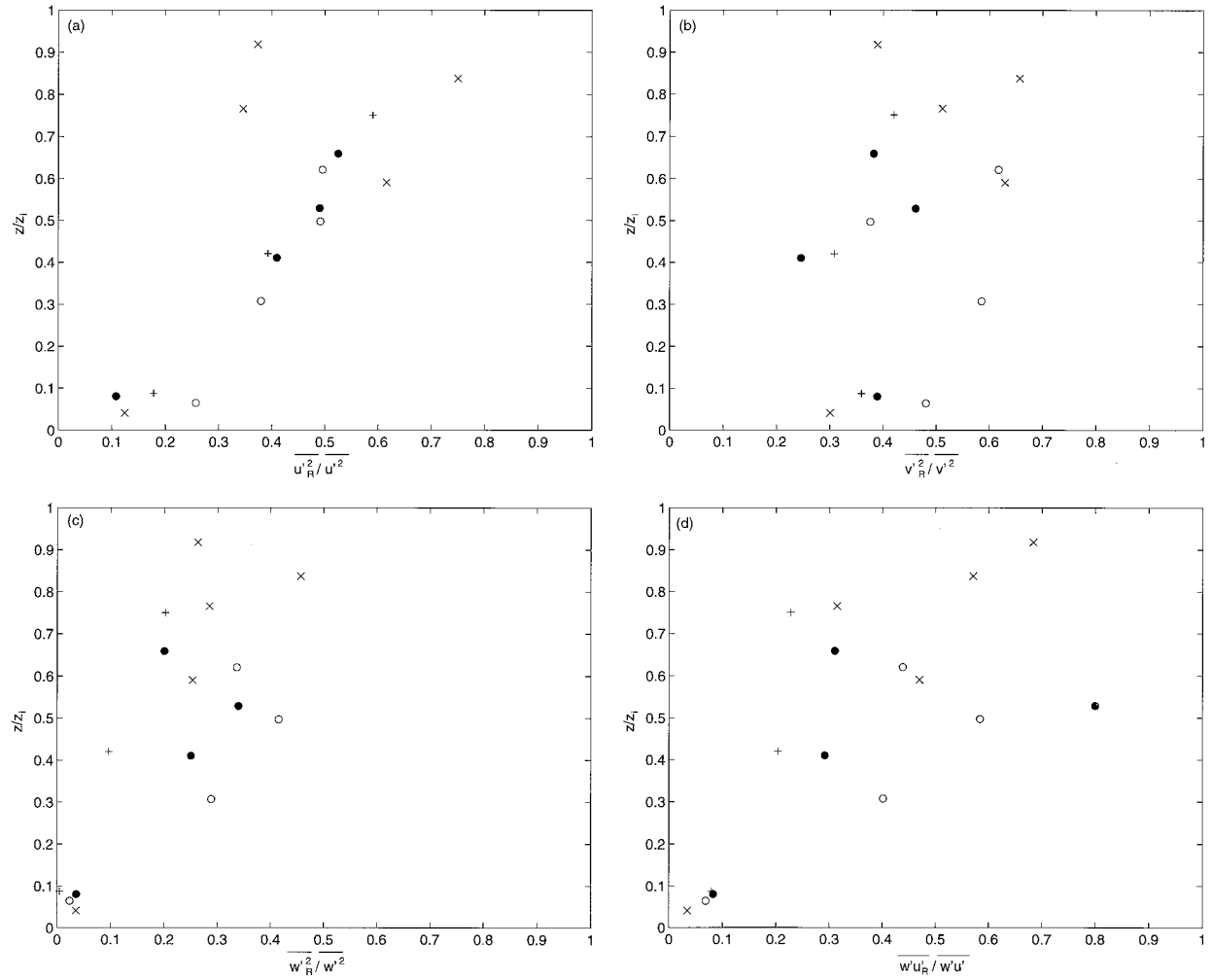

FIG. 8. Composite plots of the fractional roll-scale contributions to the velocity variances and fluxes of momentum, heat, and moisture. Individual points come from the cases (+) 9 June, (×) 16 June, (○) 21 June P3.2, and (●) 21 June P4.1. Three outlying points are indicated by their values and arrows at the appropriate altitude.

maximum near the middle of the BL. The difference between the two, the small-scale momentum flux, decreases almost linearly with altitude. The total crosswind momentum flux is more erratic, but the roll-scale contribution is consistently negative at the surface, becoming positive by about $0.25H$ and reaching a maximum near the middle of the BL. The heat and moisture fluxes show rather greater variation than the momentum fluxes or velocity variances, but it is clear that the roll scale is responsible for a significant fraction of the transport. The fractional contribution of the roll scale to the sensible heat and buoyancy fluxes increases with altitude. The contribution to the latent heat flux is difficult to assess near the surface since the total values are generally small, and errors consequently large, in the upper two-thirds of the BL the contribution is (with the exception of two points) in excess of 50% of the total flux, and most values lie between 70% and 85%.

Although the turbulence data is somewhat fragmentary, the general features of the roll-scale contributions to the velocity variances and momentum fluxes agree well with those of earlier studies (LeMone 1973; Brümmer 1985). Those of heat and moisture fluxes are less well defined and show greater variation but are consistent with the earlier results.

5. Stability parameters

In many theoretical treatments of atmospheric flows, nondimensional parameters such as the Richardson and Reynolds numbers are used to identify the stability of the flow. These have the general forms

$$\mathrm{Ri} = \frac{g}{\bar{\theta}}\frac{d\bar{\theta}/dz}{(d\bar{U}/dz)^2} \approx \frac{g}{\bar{\theta}}\frac{\Delta\bar{\theta}\Delta z}{\Delta\bar{U}^2}, \tag{5.1}$$

$$\mathrm{Re} = \frac{Uh}{K_m}, \tag{5.2}$$

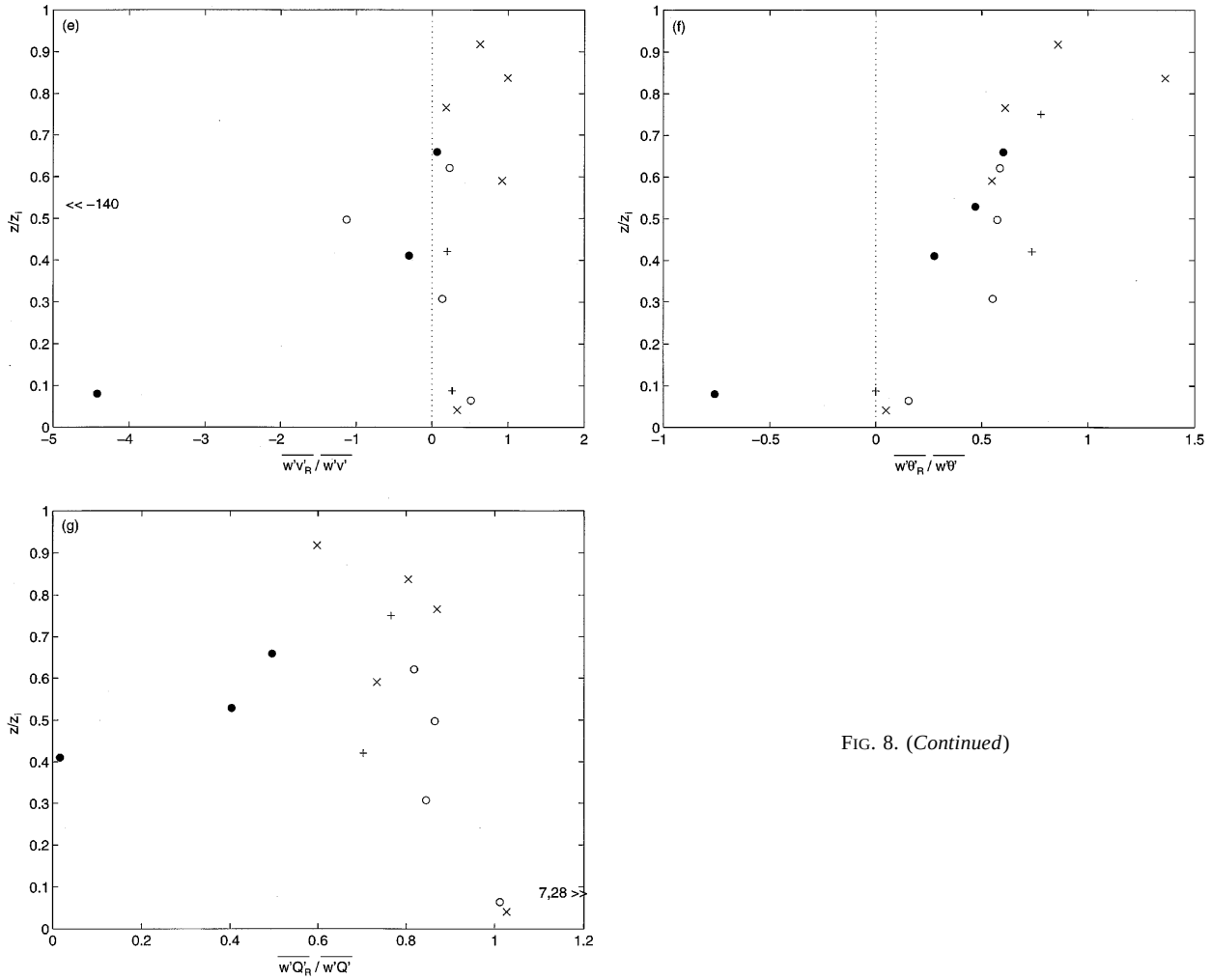

FIG. 8. (*Continued*)

where θ is usually replaced by θ_v in marine environments to account for the effects of a high moisture content on buoyancy. Here U is a velocity scale, z is altitude, h is a length scale, and K_m the turbulent viscosity. These parameters are usually defined for highly idealized profiles of temperature and wind speed and it is not always obvious how they should best be defined for the frequently much more complicated structure of observed boundary layers. It should also be borne in mind that theoretically derived results may not generalize to different definitions of these parameters used with observational data. Flows with Re greater than some critical value Re_c are dynamically unstable and may be susceptible to roll formation. Whether or not rolls will form is dependent on the relative importance of shear and buoyancy forcing and hence on the Richardson number. Under conditions of sufficiently high shear ($\mathrm{Ri} > \mathrm{Ri}_c$) the flow becomes stratified, and rolls are suppressed. At the other extreme of strong buoyancy forcing, the organization breaks down into cellular convection.

A number of different definitions for Ri and Re have been used in previous studies; we summarize some of these below. Complete definitions for the various parameters are given in Table 2. LeMone (1973) defined a bulk Richardson number with a simplified linear θ profile, defined to have the same mean θ as the observed boundary layer. The velocity gradient was taken to be the geostrophic wind speed V_g divided by the Ekman layer depth δ. To define Re, V_g and δ were also used. Kelly defined $\Delta\theta$ as the jump between the mean boundary layer θ and that equivalent to the surface water temperature. He assumed that this $\Delta\theta$ was representative of the whole BL, and since the water temperature was much greater than that of the overlying air ($\Delta\theta = 10.7$ K), the error involved in this assumption was small. The maximum BL wind speed was used to define U, and the boundary layer depth defined the length scale. Brümmer (1985) defined a number of different Richardson numbers in order to find the form that best met the theoretical condition of $\mathrm{Ri} < 0.25$ when the BL was unstable with respect to roll formation. Only one of the definitions met this condition. Here $\Delta\theta_v$ is defined as

TABLE 2. Stability parameter definitions. Some definitions of Ri and Re used by previous researchers. LeMone: $d\theta/dz$ is a linear gradient calculated so that between $z = 0$ and $z = \delta$, θ is equal to the observed value; $\bar{T}$ is the mean temperature over the Ekman layer depth; V_g is the geostrophic wind speed at the inversion; f is the Coriolis parameter; and δ is the Ekman layer depth $= (2K_m/f)^{1/2}$ estimated from the observations by LeMone as $2.84 \times$ height of maximum in roll-scale crosswind variance. Kelly: $\Delta\theta_{SL}$ is the difference between the value of θ corresponding to the water surface temperature and the mean value of θ across the mixed layer θ_{ML}; h is the inversion height; U_{BL} the maximum boundary layer wind; K_M is the coefficient of eddy momentum viscosity, assumed $= 50$ m^2 s^{-1}; Brümmer: $\Delta\theta_v$ is the difference between values of virtual potential temperature at the top of the roll layer and that corresponding to the sea surface temperature; θ_v is the mean value across the full depth of the roll layer H; u_g is the geostrophic wind, assumed equal to that just above the roll layer; $\Delta\bar{v}$ is the change in the cross-roll wind component between the surface and H; and K_m is the eddy momentum viscosity calculated from K theory (Brümmer also tried two further definitions for Ri and Re, not included here, which he judged not to be useful indicators of BL stability with respect to rolls.)

Study	Ri	Re	
LeMone (1973)	$\frac{g}{\bar{T}}\frac{d\bar{\theta}/dz}{(V_g/\delta)^2}$	$\frac{2V_g}{f\delta} = \frac{V_g\delta}{K_m}$	(a)
Kelly (1984)	$\frac{g}{\theta_{ML}}\frac{-\Delta\theta_{SL}h}{U_{BL}^2}$	$\frac{U_{BL}h}{K_m}$	(b)
Brümmer (1985)	$\frac{g}{\theta_v}\frac{\Delta\theta_v H}{u_g^2}$	$\frac{\lvert\Delta\bar{v}\rvert H}{K_m}$	(c)
		$\frac{V_g H}{K_m}$	(d)

the jump between the surface temperature and that at the top of the roll layer; the geostrophic wind speed just above the inversion was used to define the velocity scale. The θ jump used by Kelly would have been inappropriate since it would neglect the stable upper part of the less well-mixed, shear-driven BL observed. Brümmer also calculated four different Reynolds numbers, two of which are included here. The first uses the change in the cross-roll wind component between the surface and just above the roll layer as the velocity scale; the second uses the geostrophic wind speed just above the roll layer. Both definitions use the roll layer depth as the length scale.

All the Re definitions require K_m, usually assumed to be constant throughout the BL but not necessarily so. This presents an additional difficulty in the calculation of Re from observational data, since K_m must either take an assumed value, or be calculated from K theory

$$\overline{w'U'} = -K_m\frac{dU}{dz}. \tag{5.3}$$

This calculation is prone to error due to the difficulty of estimating the vertical gradient of the mean wind from an aircraft profile. The larger turbulent eddies introduce transient deviations from the mean wind that cannot be separated from genuine changes with altitude, and the shallow angle of descent results in contamination of the profile by horizontal inhomogenities. A further problem is that the time between making the vertical profile and completing the horizontal runs from which the momentum flux is calculated may be in excess of 1 h, so that we must assume conditions remain unchanged over that period. Kelly assumed a value of 50 m^2 s^{-1} for K_m, while Brümmer calculated values ranging from 15 to 35 m^2 s^{-1}. In the present study we calculate values from K theory, using the small-scale contribution to the along-wind momentum flux only. The crosswind component is found to make a negligible contribution. Values are calculated for each individual run and are generally found to decrease with altitude; however, a single mean value has been used in the calculation of Re. Mean values range from 3 to 12.6 m^2 s^{-1}, smaller than those of Kelly and Brümmer, as expected for the less convective conditions.

Conditions in the present study are broadly similar to those of Brümmer (1985) though, in general, with even less buoyancy forcing. We have adopted his favored definition of Ri with one minor modification; low-level value of θ_v used is that from the bottom of the profile, at 14 m, rather than the value equivalent to the SST. Two reasons contributed to this choice of modification. First, because of the SST gradients off the California coast, a mean SST determined during a low-level flight leg might differ slightly from the value in the vicinity of the profile, perhaps 10 km or more away. Second, and more importantly, a number of the profiles we wished to include in the stability analysis had no associated horizontal runs from which SSTs might be determined. The measurement of SST during vertical profiles is unreliable due to the temperature dependence of the radiometer used.

Table 3 lists values of Ri and Re for all the cases studied, along with values of z_i/L and u_*/w_* where near surface turbulence runs were available; also listed are the values of parameters used in the calculations. The Richardson numbers are in excellent agreement with the observations of rolls. In all cases where rolls were observed, Ri < 0.25. The exact value of Ri reflects to some extent the strength of the rolls. Where Ri < 0.1, the rolls have been most easily visible in the crosswind turbulence runs. As Ri increases it generally becomes more difficult to identify the presence of roll from the turbulence data alone. For example, the 8 June case has Ri $= 0.15$, which would suggest that the BL may be unstable with respect to the formation of rolls, but the turbulence data was ambiguous and cloud cover too sparse for us to confidently decide whether or not rolls were present. A few tens of kilometers closer to the coast, however, cloud streets were visible, and it seems plausible that our observations were made in a transitional region between rolls and the disorganized, broken cloud field observed farther from the coast. For the case on 21 June (P4.1), the turbulence data led to the tentative conclusion that weak rolls were present, consistent with

TABLE 3. Stability parameters. Here, L is the Obukhov length; u^* and w^* are the friction and convective velocities, respectively, both determined for horizontal flight legs at 30 m; Ri is the bulk Richardson number; and Re(a–d) are Reynolds numbers (defined in Table 2). Where there has been some uncertainty as to the exact values to use in calculating the stability parameters, a range of values is indicated. Also given are the parameters used to calculate Ri and Re: the mean and jump in θ_v, the jump in the crosswind velocity v, the geostrophic wind U_g (assumed equal to the mean wind speed just above the inversion), and the turbulent viscosity K_m. Also required is the Coriolis parameter, which has a value of approximately 8.5×10^5. Where an entry is blank data is unavailable, a dash indicates that a parameter is not applicable.

Date	Rolls?	Z_i/L	u^*/w^*	Ri	Re (a)	Re (b)	Re (c)	Re (d)	$\bar{\theta}v$	$\Delta\theta v$	$\lvert\Delta v\rvert$	U_g	K_m
08:P2	?	−0.6	0.87	0.15	1325	2726	58 (230)	2900	288.1	1.7	0.3 (1.2)	15	3
09:P1	Y	−0.5	0.92	0.03	1327	1739	>134	1647	288.4	0.7	3.5	16	3.4
11:P1	N			0.3					288.9	1.8	0.75 (0.5–1)	10	
16:P1	Y	−2.3	0.55	0.04	698	896	66	942	286.5	0.4	1.1–1.6	16	12.3
17:P1	Y	−0.16	1.38	0.13	1026	2037	195	1830	286.8	1.6	3.2	15	5
21:P3.2	Y	−0.9	0.75	0.05	388	583	55	882	287.1	0.3	1.5	9	12.6
21:P4.1	Y	−0.06	1.67	0.17	785	816	<27	707	285.8	2.3	0–0.5	13	6.8
22:P2	Y			<0.1					286.8	1.3	3.2	15	
22:P3	Y			0.08					286.7	0.7	2	12	
22:P4	Y			0.08					286.8	0.5	2.2	11	
22:P5	N			0.27					287.0	1.0	1.5	9	
27:P2	N	0.3	—	0.3	485	717	114	520	288.3	1.8	2.2	10	10
28:P2	N	−1.6	0.62	0.5	485	870	70	645	287.9	2.5	1.1	10	10

a value of Ri = 0.17. In all the cases without rolls we find Ri > 0.25.

Four different Reynolds numbers are listed: Re(a–d) correspond to the definitions of LeMone (1973), Kelly (1984), and Brümmer (1985) listed in Table 2. Values for Re(a, b, d) are all large, reflecting the shear-dominated flow and dynamic instability. Here, Re(d) is perhaps the most appropriate definition since it uses the same length and velocity scales as Ri. Reynolds number Re(c) stands out as having much lower values than the other definitions. Brümmer and Latif (1985) used this definition in a linear perturbation analysis of the inflection point instability in a neutral BL. They found that for Re(c) < Re_c the dynamic instability did not operate, where Re_c had a minimum of 50 for an inflection point near the middle of the BL and increased as the inflection point moved up or down. Brümmer (1985) applied this finding to assign a dominant mechanism to each of his roll cases. It is not obvious whether this result should apply to the cases presented here, where any inflection points are close to the inversion and the flow may be heavily modified from the preroll conditions. The criterion would suggest that the cases on 21 June (P4.1), and possibly 16 and 21 June (P3.2) are not dynamically forced. The high wind speed and small buoyancy fluxes make this conclusion questionable. Figure 9 shows the contributions to the roll-scale kinetic energy budget from buoyancy, and the across- and along-roll wind

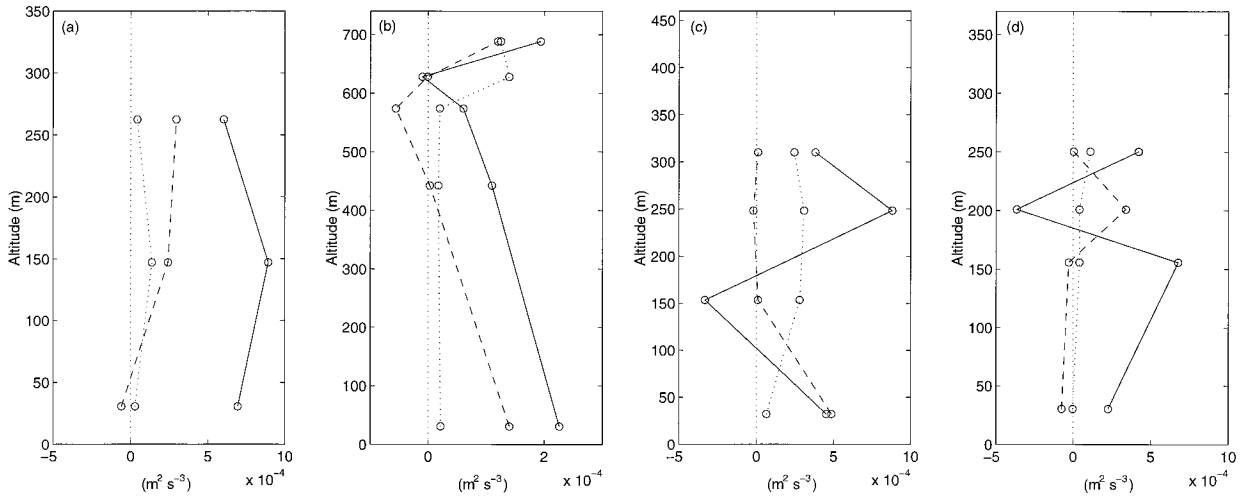

FIG. 9. The buoyancy and shear terms in the roll-scale kinetic energy budget for cases on (a) 9 June, (b) 16 June, (c) 21 June P3.2, and (d) 21 June P4.1. The solid lines are the along-wind shear terms $-\overline{w_R u_R}\,d\bar{u}/dz$, dashed lines the crosswind shear terms $-\overline{w_R v_R}\,d\bar{v}/dz$, and the dotted lines the buoyancy terms $(g/\bar{\theta}_v)\overline{w'\theta_v'}$. Note that the along-wind term contributes only to the rate of change of kinetic energy parallel to the roll axis.

components. The problem of estimating accurate vertical gradients of the wind components noted earlier apply here also, and the shear terms should be regarded with some caution. In general, both the cross-roll wind shear and the buoyancy contribute positively to the roll energy, although not through the whole of the BL depth. It is noted that in support of Brümmer and Latif's (1985) Re criterion, the cross-roll shear term is negative in the lower BL on 21 June (P4.1). Near the middle of the BL, however, it has a much larger positive contribution, while the buoyancy contribution is positive but small throughout the BL.

6. Summary and conclusions

We have determined a stability parameter in the form of a bulk Richardson number for each of thirteen profiles through near neutral boundary layers off the coast of California. The Richardson number accurately predicts the presence of BL spanning rolls, assuming a critical value of approximately 0.25. Where rolls were clearly identified by independent observations, we found $\mathrm{Ri} < 0.1$ and $\mathrm{Ri} \approx 0$ where the rolls were strongest. For $0.1 < \mathrm{Ri} < 0.25$ rolls were weak with poor coherence over large scales. No rolls were observed in cases where $\mathrm{Ri} > 0.25$. Near the shear limit of the range of roll supporting conditions the Richardson number provides a more accurate indication of rolls than z_i/L. For example, on 28 June $z_i/L = -1.6$, which meets Moeng and Sullivan's (1994) condition for rolls; however, $\mathrm{Ri} = 0.5$, accurately predicting that there are no BL spanning rolls. Conversely, on 21 June both of the cases studied have values of z_i/L outside any of the reported ranges for rolls: -0.9 and -0.06 for profiles P3.2 and P4.1, respectively. Here, Ri has the values 0.05 and 0.17, accurately reflecting the existence of rolls in both cases. No data are available under conditions near the buoyancy limit of the range of roll conditions. It seems likely, however, that the Richardson number may fail as a useful indicator for rolls under conditions of strong buoyant forcing. In the extreme case of an unstable boundary layer, the term $\Delta\theta_v$ may become negative and $\mathrm{Ri} < 0.25$ whether or not rolls existed. Under strongly convective conditions the definition of the upper boundary from which $\Delta\theta_v$ is evaluated becomes more critical since convective clouds may penetrate farther up the inversion and cloud top will no longer be coincident with the inversion base. We should emphasize that critical values of a stability parameter such as Ri may be dependent on the precise definition chosen. It is thus probable that other definitions of Ri will have a different critical value with respect to rolls or may even be insensitive to their presence. Thus, our results may not generalize to other definitions of the Richardson number. Further testing for both roll and nonroll cases is desirable for a wider range of ambient conditions. It should also be noted that the use of the 14-m value of θ_v rather than a surface value will lead to a small change in the values of Ri calculated and hence of the critical value. We estimate that close to the critical value, our quoted values are approximately 15% higher than if calculated with θ_v for saturated air at the SST.

Reynolds numbers have been calculated from four different definitions. Three of these give comparable, large values indicating the dynamic instability of the shear dominated flow. The fourth definition, Re(c), includes only the cross-roll wind shear and gives much lower values. Brümmer (1985) used this definition to differentiate between rolls due to dynamic and thermal instabilities, but its applicability to our observations is not obvious.

Estimates of the shear and buoyancy contributions to the roll-scale kinetic energy budget suffer from large errors associated with the determination of the vertical gradients of the wind speed and a relatively small number of data points, and must be considered inconclusive.

For four of the roll cases detailed turbulence measurements were available from stacks of straight and level, crosswind flight legs. The roll-scale contribution to the total velocity variances and turbulent fluxes of sensible and latent heat, and momentum have been determined for these cases. The u and w variances, and the sensible heat, and along-wind momentum fluxes all show a near linear increase in the fractional contribution from rolls with altitude, from less than 0.1 at 30 m to 0.7–1 at the top of the BL. The variance in v and cross-wind momentum flux are very much more scattered, although the variance shows a slight increase with altitude, from about 0.3 to 0.6 across the BL depth. The latent heat flux also shows a great deal of scatter, especially in the lower third of the BL, largely due to the near zero moisture fluxes near the surface; above this values range between about 0.4 and 0.85 but show no clear trends.

Acknowledgments. This work was supported by the Office of Naval Research through Grants N00014-93-1-0972 and N00014-95-1-0857. We would like to thank the Royal Air Force crew of the C-130 *Hercules* and the support scientists from MRF for their work during the field project. The satellite image in Fig. 1 was provided by the Remote Sensing Laboratory at the Naval Postgraduate School, Monterey. We are grateful to three anonymous reviewers; their careful reading and detailed comments have helped greatly to improve the paper.

REFERENCES

Brost, R. A., D. H. Lenschow, and J. C. Wyngaard, 1982: Marine stratocumulus layers. Part I: Mean conditions. *J. Atmos. Sci.,* **39,** 800–817.

Brown, R. A., 1980: Longitudinal instabilities and secondary flows in the planetary boundary layer: A review. *Rev. Geophys. Space Phys.,* **18,** 683–697.

Brümmer, B., 1985: Structure, dynamics and energetics of boundary layer rolls from KonTur aircraft observations. *Beitr. Phys. Atmos.,* **58,** 237–254.

——, and M. Latif, 1985: Some studies on inflection point instability. *Beitr. Phys. Atmos.,* **58,** 117–126.

——, H. Schlünzen, and W. Bögel, 1982: Cloud streets during KonTur. *KonTur Convection and Turbulence Experiment. Preliminary Scientific Results,* Hamburger Geophys. Einzelschriften. Part A: Wissenschaftliche Abhandlungen, Vol. 57, Max-Planck Institute For Meteorology, 63–77.

Chlond, A., 1992: Three-dimensional simulation of cloud street development during a cold air outbreak. *Bound.-Layer Meteor.,* **58,** 161–200.

Chou, S.-H., 1993: A comparison of airborne eddy correlation and bulk aerodynamic methods for ocean-air turbulent fluxes during cold air outbreaks. *Bound.-Layer Meteor.,* **64,** 75–100.

——, and J. Zimmerman, 1989: Bivariate conditional sampling of buoyancy flux during an intense cold-air outbreak. *Bound.-Layer Meteor.,* **46,** 93–112.

——, and M. P. Ferguson, 1991: Heat fluxes and roll circulations over the western gulf stream during an intense cold-air outbreak. *Bound.-Layer Meteor.,* **55,** 255–281.

Deardorff, J. W., 1972: Numerical investigation of neutral and unstable planetary boundary layers. *J. Atmos. Sci.,* **29,** 91–115.

Etling, D., and R. A. Brown, 1993: Roll vortices in the planetary boundary layer: A review. *Bound.-Layer Meteor.*, **65,** 215–248.

Glendening, J. W., 1996: Lineal eddy features under strong shear conditions. *J. Atmos. Sci.,* **53,** 3430–3449.

Hein, P. F., and R. A. Brown, 1988: Observations of longitudinal roll vortices during arctic cold air outbreaks over open water. *Bound.-Layer Meteor.,* **45,** 177–199.

Kelly, R. D., 1984: Horizontal roll and boundary-layer interrelationships observed over Lake Michigan. *J. Atmos. Sci.,* **41,** 1816–1826.

LeMone, M. A., 1973: The structure and dynamics of horizontal roll vortices in the planetary boundary layer. *J. Atmos. Sci.,* **30,** 1077–1091.

——, 1976: Modulation of turbulence energy by longitudinal rolls in an unstable planetary boundary layer. *J. Atmos. Sci.,* **33,** 1309–1320.

Martin, G. M., D. W. Johnson, D. P. Rogers, P. R. Jonas, P. Mannis, and D. A. Hegg, 1995: Observations of the interaction between cumulus clouds and warm stratocumulus clouds in the marine boundary layer during ASTEX. *J. Atmos. Sci.,* **52,** 2902–2922.

Moeng, C.-H., and P. P. Sullivan, 1994: A comparison of shear- and buoyancy-driven planetary boundary layer flows. *J. Atmos. Sci.,* **51,** 999–1022.

Raasch, S., 1990: Two numerical case studies of horizontal roll vortices in near-neutral inversion capped planetary boundary layers. *Beitr. Phys. Atmos.,* **63,** 205–222.

Rogers, D. P., and J. W. Telford, 1986: Metastable stratus tops. *Quart. J. Roy. Meteor. Soc.,* **112,** 481–500.

——, and D. Koracin, 1992: Radiative transfer and turbulence in the cloud-topped marine atmospheric boundary layer. *J. Atmos. Sci.,* **49,** 1473–1486.

——, D. W. Johnson, and C. A. Friehe, 1995: The stable internal boundary layer over a coastal sea. Part I: Airborne measurements of the mean and turbulence structure. *J. Atmos. Sci.,* **52,** 667–683.

Sykes, R. I., and D. S. Henn, 1989: Large-eddy simulation of turbulent sheared convection. *J. Atmos Sci.,* **46,** 1106–1118.

Walter, B. A., and J. E. Overland, 1984: Observations of longitudinal rolls in a near neutral atmosphere. *Mon. Wea. Rev.,* **112,** 201–208.

Woodcock, A., 1941: Soaring over the open sea. *Sci. Mon.,* **25,** 226–232.